# High-NA optical edge detection via optimized multilayer films

Wenjin Xue[1] and Owen D. Miller[2]

[1] *Department of Electrical Engineering and Energy Sciences Institute, Yale University, New Haven, Connecticut 06511, USA*
[2] *Department of Applied Physics and Energy Sciences Institute, Yale University, New Haven, Connecticut 06511, USA*

(Dated: January 11, 2021)

There has been a significant effort to design nanophotonic structures that process images at the speed of light. A prototypical example is in edge detection, where photonic-crystal-, metasurface-, and plasmon-based designs have been proposed and in some cases experimentally demonstrated. In this work, we show that multilayer optical interference coatings can achieve visible-frequency edge detection with high numerical aperture, two-dimensional image formation, and straightforward fabrication techniques, unique among all nanophotonic approaches. We show that the conventional Laplacian-based transmission spectrum may not be ideal once the scattering physics of real designs is considered, and show that better performance can be attained with alternative spatial filter functions. Our designs, comprising alternating layers of Si and $SiO_2$ with total thicknesses of only $\approx 1\,\mu m$, demonstrate the possibility for optimized multilayer films to achieve state-of-the-art edge detection, and, more broadly, analog optical implementations of linear operators.

In this article, we show that optimally designed multilayer dielectric films can achieve high-numerical-aperture optical edge detection. In a typical scenario, one might have a scene or object illuminated by a laser or narrow-bandwidth source, in which case an optical device that generates an image of edges offers the prospect for speed-of-light detection [1–9]. Of the many edge-detection designs to date [2–9], none offers all three of: high numerical aperture, two-dimensional image formation, and the prospect for realistic fabrication. Multilayer films are commonly fabricated to high precision for wide-ranging applications [10, 11], and guarantee a two-dimensional field of view by their rotational symmetry. Thus the key question is whether they can achieve high-fidelity edge detection for a large numerical aperture, which we show is indeed possible with geometrical optimization. The canonical approach to achieving edge-detection behavior [12, 13] is to target a transmission profile that scales with $k_\rho^2$, for in-plane wavenumber $k_\rho$, as such a profile will mimic the effect of the in-plane Laplacian operator, $\nabla_\perp^2$ on the incoming field. We show that targeting such a quadratic profile with a multilayer structure can successfully produce an effective design. Yet, the design is imperfect, and the requirement of a $k_\rho^2$ profile is an overprescription of the response function. *Any* transmission response that acts as a high-pass filter, i.e., which filters out small wavenumbers (corresponding to nearly constant in-plane spatial modes), can produce high-quality edges. To demonstrate this, we show that a transmission profile that scales as the *cube* of the incident angle, $\sim \theta^3$, can produce even higher-quality images for the same design parameters. Our designs offer the highest theoretical performance to date, should be straightforward to fabricate, and reveal the potential of such multilayer structures for analog optical devices.

The essential feature of optical analog edge detection, as shown in Fig. 1, is to engineer the light field of a coherent image, isolating its edges in the transmission or reflection spectrum of an optical device. A classic approach [14] to analog edge detection is to use a lens to Fourier transform the incoming waves and an aperture to filter out the low-wavenumber components, with two free-space propagation regions to allow the evolution of the wave field to achieve the Fourier and Inverse-Fourier Transforms. The key drawback is that the setup must be large and bulky to accommodate the free-space propagation. An emerging alternative is to use coherent scattering effects to isolate edges in a more compact device architecture, including photonic-crystal slabs [3, 8, 9], dielectric metasurfaces [5–7], plasmonic films [2], and split-ring-resonator metamaterials [4]. The incoming field, for a given polarization at a frequency of interest, can be written as a linear combination of plane waves, $\int E_{\text{in}}(k_\rho) e^{i(k_\rho \rho + k_z z)}\, \mathrm{d}k_\rho$. One method to identify edges is to try to identify a structure whose wavenumber-dependent transmission or reflection mimics the in-plane Laplacian operator, $\nabla_\perp^2$. In the spatial Fourier space, the Laplacian corresponds to multiplying the incoming

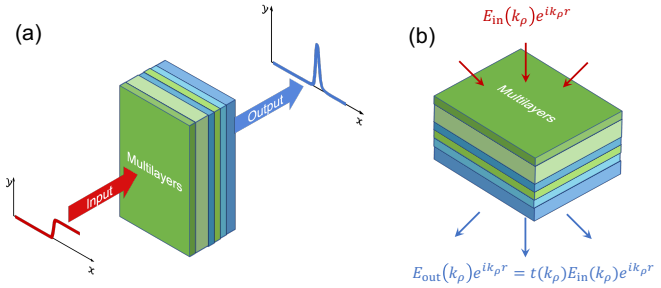


FIG. 1. (a) Illustration of edge detection with multilayer films. (b) Edge detection can be achieved by engineering the transmission spectrum in Fourier space. For a coherent incident wave decomposed into its plane-wave constituents, labeled by in-plane wavenumber $k_\rho$, the transmission coefficient $t(k_\rho)$ determines the image at the output plane.

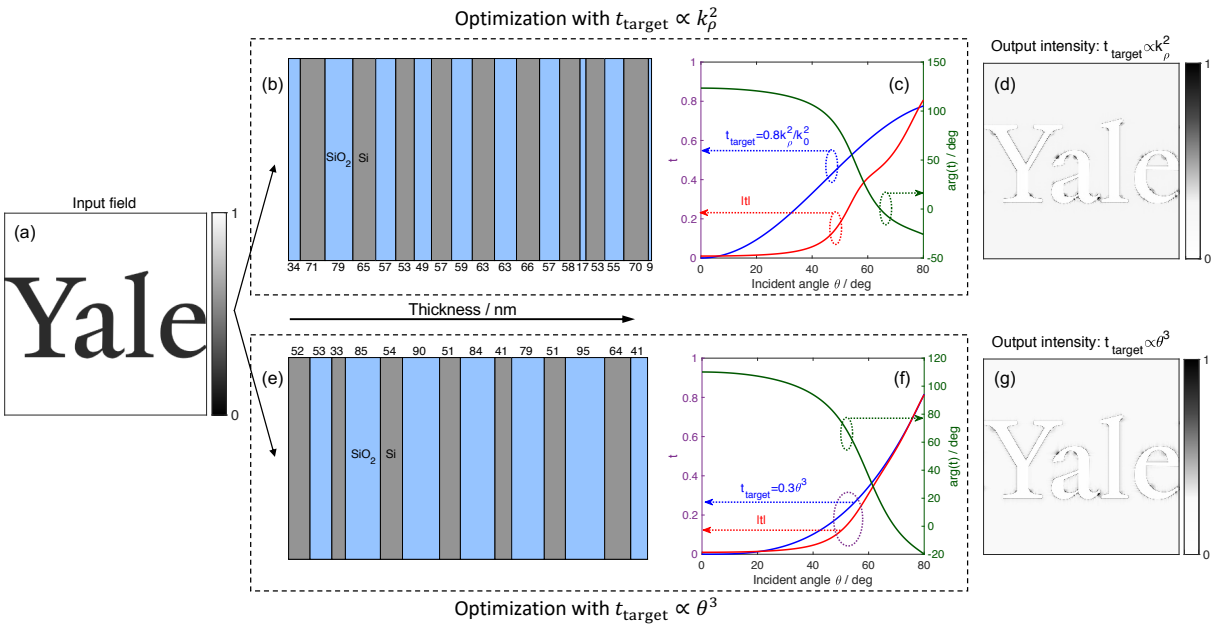


FIG. 2. Multilayer edge-detection designs for operating wavelength of 700 nm. (a) Input image, with edges oriented in every direction. (b) Optimal design for a target transmission coefficient proportional to the square of the wavenumber. The design comprises alternating layers of Si and $SiO_2$. (c) Transmission coefficients, in magnitude and phase, of the target and optimal designs, showing close but imperfect correspondence. (The target design has phase 0 at all $\theta$.) (d) Output image, clearly showing edges and with minimal background noise or interference. (e-g) Same plots as (b-d) but not for a target transmission coefficient proportional to the cube of the incident angle, demonstrating that other spatial filter functions can demonstrate as good or better performance as the quadratic Laplacian spectrum.

plane waves by $k_\rho^2$, suppressing low spatial frequencies relative to high ones. The effectiveness of the Laplacian can be attributed to the fact that edges are high-spatial-frequency components of images, whereas a low-contrast background comprises primarily low spatial frequencies. Although the devices discussed above [2–9] have shown the possibility for discriminating edges within an image, there have been key drawbacks to each approach: they have been limited to one-dimensional (or partial-two-dimensional) image formation, they have had limited numerical aperture, and/or they have comprised hard-to-fabricate structures.

Multilayer films (i.e., optical interference coatings) have well-established fabrication techniques [15, 16], and their optical response is necessarily isotropic under rotations around their propagation axis. Thus if their transmission coefficients can be optimized to have the right profile, they can simultaneously satisfy the three key requirements (high NA, 2D field of view, and simple fabrication). We define a target transmission coefficient, $t_{\text{target}}$, as a function of angle (or, equivalently, wavenumber), which serves as the ideal transmission function for edge detection. We take the allowed materials in the multilayer to be given, and use the *widths* of the corresponding layers, $w_\ell$ for each layer $\ell$, to be the designable degrees of freedom. Our optimization problem, then, is:

$$\min_{w_\ell} \sum_\theta |t(\theta; w_\ell) - t_{\text{target}}(\theta)|^2 \qquad (1)$$

where $t(\theta; w_\ell)$ is the transmission coefficient of a given multilayer stack. One can optimize the transmission coefficient for edge-image formation at any output plane beyond the multilayer; to demonstrate how compact this approach can be, we take the image plane to be the exterior of the rear surface itself.

For optimization of a large number of layers, one must be able to rapidly compute gradients of the objective function, Eq. (1), with respect to the many degrees of freedom. Here we briefly outline how the gradients are computed, using a method similar to that of the "needle" approach to multilayer-film design [17–20]. In a multilayer medium, the continuous translational and rotational symmetry prevents coupling between different wavenumbers. At each wavenumber, the standard matrix approach [10] connects the forward- and backward-going wave amplitudes in the incident region to the equivalent amplitudes in the transmission region through matrices $P_\ell$ and $D_\ell$ and that represent propagation through, and interface reflections at, layer $\ell$. The reflection coefficient $r$ and transmission coefficient $t$ satisfy the matrix equa-

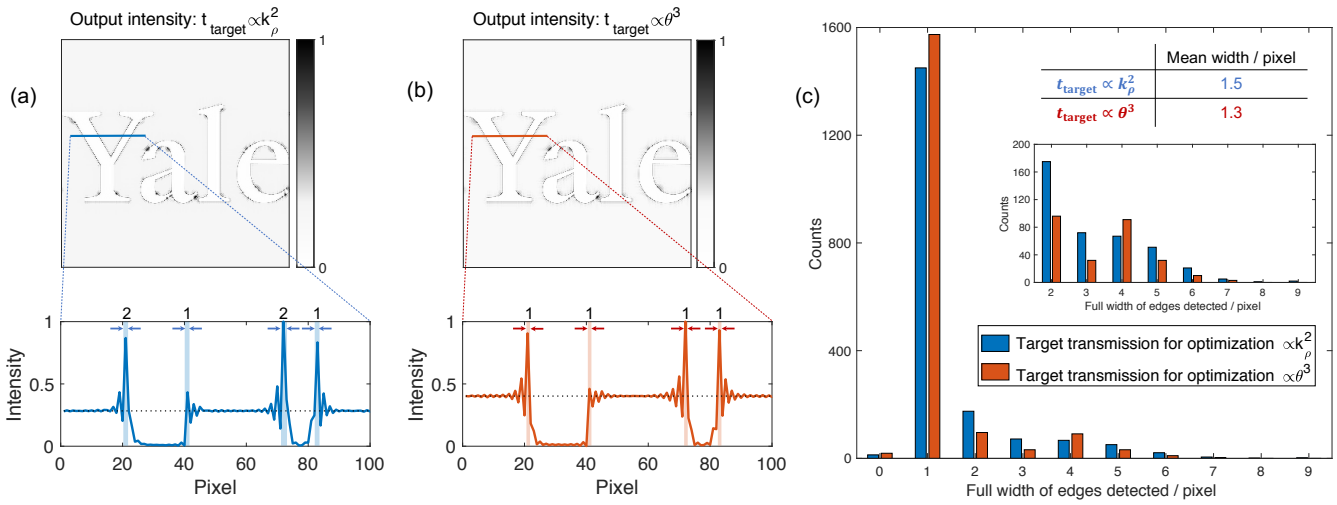


FIG. 3. Width distributions of the detected edges for the two target transmission coefficients depicted in Fig. 2. (a,b) Output images (top) and distributions of edges along an example line (bottom) for (a) $t_{\text{target}} \propto {k_\rho}^2$ and (b) $t_{\text{target}} \propto \theta^3$, respectively. The edge widths are defined as the widths over which the intensity surpass the noise level. (c) Histogram of widths in each approach, showing that the cubic-in-angle target coefficient yields slightly better results, i.e., narrower edges, than the quadratic-in-wavenumber target coefficient. Non-quadratic target functions can be superior when accounting for the scattering properties of real physical implementations.

tion [10]:

$$\begin{pmatrix} 1 \\ r \end{pmatrix} = D_0^{-1} \left[ \prod_{\ell=1}^{N} D_\ell P_\ell D_\ell^{-1} \right] D_s \begin{pmatrix} t \\ 0 \end{pmatrix} = \begin{pmatrix} M_{11} & M_{12} \\ M_{21} & M_{22} \end{pmatrix} \begin{pmatrix} t \\ 0 \end{pmatrix}. \quad (2)$$

where the "1" on the left-hand side represents the incident-wave normalization, and the reflection coefficient, transmission coefficient, and the matrices $P_\ell$ and $D_\ell$ all vary with wavenumber $k_\rho$. One can then solve for $r$ and $t$ from the components of the $M$ matrix; in particular, $t$ is given by $t = 1/M_{11}$. The derivative of $t$ with respect to the width of region $i$ is then given by $\mathrm{d}t/\mathrm{d}w_i = -(1/M_{11}^2)\mathrm{d}M_{11}/\mathrm{d}w_i$. A change in the width of layer $i$ does not affect interface transmission and reflection, and will only incur changes in the propagation matrix $P_i$ in the product of Eq. (2). The derivative of the $M$ matrix can then be written:

$$\frac{\mathrm{d}M}{\mathrm{d}w_i} = D_0^{-1} \left[ \prod_{\ell=1}^{i-1} D_\ell P_\ell D_\ell^{-1} \right] D_i \frac{\mathrm{d}P_i}{\mathrm{d}w_i} D_i^{-1} \left[ \prod_{\ell=i+1}^{N} D_\ell P_\ell D_\ell^{-1} \right] D_s \quad (3)$$

which can be rapidly computed.

Figure 2 demonstrates the capability for high-efficacy edge detection with a computationally optimized multilayer stack. We consider up to 20 alternating layers of Si and $SiO_2$, with refractives indices $3.77 + 0.01i$ and 1.47, respectively, for p-polarized light incident at 700 nm wavelength. To perform the optimization, we use the gradient computed via Eq. (3) in a local, gradient-based interior-point method [21–24] that is run until convergence. Simulations of image formation are done by Fourier transforming the incident field, multiplying by the wavenumber-dependent transmission, and then inverse Fourier transforming at the output plane. As our input we consider a Yale logo, containing edges oriented in almost every direction. We take the image to occupy a numerical aperture of $\approx 0.98$, corresponding to polar angles ranging from 0° to 80°.

In one set of optimizations, we targeted a Laplacian-based transmission coefficient function given by $t_{\text{target}}(\theta) = \alpha k_\rho^2$, where $\alpha$ is a constant optimization hyperparameter. After running the optimization over many different values of $\alpha$ and many initialization points for the layer widths, the design shown in Fig. 2(b), slightly more than 1 µm in total thickness, emerged as optimal. Figure 2(c) shows the actual transmission coefficient of the design (red and green lines), compared to the target (blue). The targeted quadratic $k_\rho^2$ distribution is not exactly achieved, but the variation in phase is less than $\pi$ over the whole angular range, which ensures effective interference at the image plane. The intensity of the output field is shown in Fig. 2(d), where one can see that the edges, oriented in all directions, are clearly resolvable.

As mentioned in the introduction, edge detection requires good filtering of the spatial frequencies of the incoming wave, but such filtering does *not* necessarily re-

quire the $k_\rho^2$ dependence of the Laplacian operator. The discrepancy between the optimal-design transmission coefficient and that of the target in Fig. 2(c) suggests that it may be impossible for multilayer structures to achieve perfect quadratic scaling of their transmission coefficients alongside minimal phase variations, which would imply that the optimal design of Fig. 2(b) may have paid some penalty in attempting to minimize the difference with a quadratic target, instead of simply aiming for good filtering properties.

In Fig. 2(e), we show an alternative design that emerged for a target transmission coefficient given by $t_{\text{target}}(\theta) = \alpha\theta^3$. We chose this function to more closely match the transmission curves of real multilayer designs, and Fig. 2(f) shows the much closer match between the transmission coefficient of the new optimal design and that of the new target. In Fig. 2(g) the output-field intensity again shows very good edge resolution, although it is difficult by eye to detect which of the designs of Fig. 2(b,e) is better.

Figure 3 quantitatively compares the edge image quality of the two designs of Fig. 2(b,e). We measure the width of every edge that is present in the output, and compare between the two designs (also using the ground truth that is known from the input image). Figure 3(a,b) demonstrates prototypical results, where the design using $k_\rho^2$ target transmission exhibits thicker edges, as measured by the number of pixels above the background intensity (dashed lines), than its counterpart designed with $t_{\text{target}} \sim \theta^3$. The histogram of Fig. 3(c) shows the relative numbers of edges with a given width (in terms of number of pixels) for the two designs, with the $\theta^3$ design offering slightly better performance and a lower average width per pixel. (The number of edges missed entirely is nonzero but very small for both designs.) This demonstrates that, although the Laplacian operator may be a good starting point for edge-detection design, it is neither required nor necessarily globally optimal.

In Fig. 4 we compare the multilayer designs of Fig. 2(b,e) to other recent state-of-the-art designs [2–9]. The designs in the upper (grey) half of the figure all have rotational symmetry, under continuous or discrete rotations, that make their scattering response independent (or nearly so) of azimuthal angle. Of these designs, three [2, 3, 8] operate only for low numerical aperature (which corresponds to operation over only a narrow range of wavenumbers), while the fourth [4] is difficult or impossible to fabricate. The optimized multilayer films of this work show a clear advantage along these three dimensions.

Looking forward, computational optimization of multilayer structures may enable a wide range of analog linear operators, beyond just edge detection. Instead of defining specific target transmission coefficient profiles, as in Eq. (1), one could utilize a data-driven approach that matches the desired features in a given scattered field with those of known image/field pairs. We did implement such an approach for the edge detection problem, but the performance of the optimal designs was nearly equivalent to the best designs already shown here. Another possible direction to explore is towards significantly thicker multilayer designs, which may enable efficient multi-polarization and/or multi-frequency performance, though in such a case local-optimization techniques might falter and require global-optimization techniques instead.

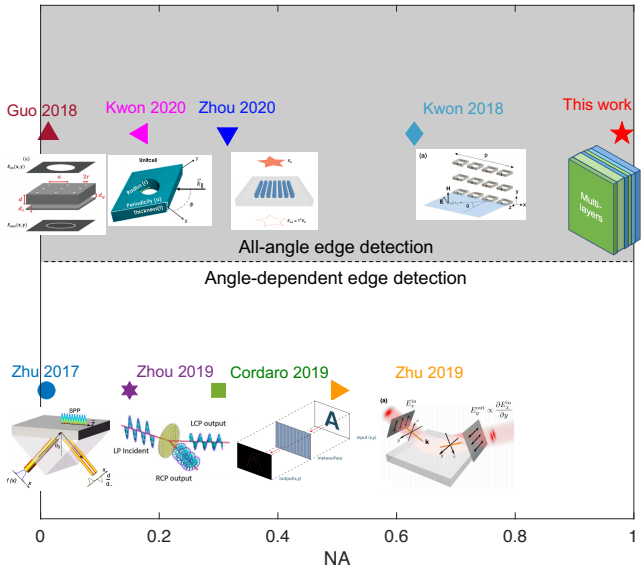


FIG. 4. Comparison of the multilayer designs to alternative, recently proposed designs [2–9]. The gray region indicates structures that effectively detect edges in two-dimensional images, while structures in the white region achieve partial-2D detection or detect edges along one-dimensional lines. Multilayer-designs show uniquely strong capabilities along the three key features of two-dimensional image formation, high numerical aperture (0.98 in this work), and feasibility of fabrication.

*Acknowledgments*—The authors thank Francesco Monticone for useful discussions. This work was supported by the Air Force Office of Scientific Research under award number FA9550-17-1-009.

[1] D. R. Solli and B. Jalali, Analog optical computing, Nature Photonics **9**, 704 (2015).
[2] T. Zhu, Y. Zhou, Y. Lou, H. Ye, M. Qiu, Z. Ruan, and S. Fan, Plasmonic computing of spatial differentiation, Nature communications **8**, 1 (2017).
[3] C. Guo, M. Xiao, M. Minkov, Y. Shi, and S. Fan, Photonic crystal slab laplace operator for image differentiation, Optica **5**, 251 (2018).
[4] H. Kwon, D. Sounas, A. Cordaro, A. Polman, and A. Alù, Nonlocal metasurfaces for optical signal process-

ing, Physical review letters **121**, 173004 (2018).
[5] T. Zhu, Y. Lou, Y. Zhou, J. Zhang, J. Huang, Y. Li, H. Luo, S. Wen, S. Zhu, Q. Gong, *et al.*, Generalized spatial differentiation from the spin hall effect of light and its application in image processing of edge detection, Physical Review Applied **11**, 034043 (2019).
[6] J. Zhou, H. Qian, C.-F. Chen, J. Zhao, G. Li, Q. Wu, H. Luo, S. Wen, and Z. Liu, Optical edge detection based on high-efficiency dielectric metasurface, Proceedings of the National Academy of Sciences **116**, 11137 (2019).
[7] A. Cordaro, H. Kwon, D. Sounas, A. F. Koenderink, A. Alù, and A. Polman, High-index dielectric metasurfaces performing mathematical operations, Nano letters **19**, 8418 (2019).
[8] Y. Zhou, H. Zheng, I. I. Kravchenko, and J. Valentine, Flat optics for image differentiation, Nature Photonics **14**, 316 (2020).
[9] H. Kwon, A. Cordaro, D. Sounas, A. Polman, and A. Alu, Dual-polarization analog 2d image processing with nonlocal metasurfaces, ACS Photonics **7**, 1799 (2020).
[10] P. Yeh *et al.*, *Optical waves in layered media*, Vol. 95 (Wiley New York, 1988).
[11] J. Faist, F. Capasso, D. L. Sivco, C. Sirtori, A. L. Hutchinson, and A. Y. Cho, Quantum cascade laser, Science **264**, 553 (1994).
[12] A. Silva, F. Monticone, G. Castaldi, V. Galdi, A. Alù, and N. Engheta, Performing mathematical operations with metamaterials, Science **343**, 160 (2014).
[13] P. H. Lissberger, Optical applications of dielectric thin films, Reports on Progress in physics **33**, 197 (1970).
[14] J. W. Goodman, *Introduction to Fourier optics* (Roberts and Company Publishers, 2005).
[15] R. C. Jaeger, *Introduction to microelectronic fabrication*, Vol. 2 (Prentice Hall Upper Saddle River, NJ, 2002).
[16] K. Seshan, *Handbook of thin film deposition processes and techniques* (William Andrew, 2001).
[17] C. vd Laan and H. Frankena, Fast computation method for derivatives of multilayer stack reflectance, Applied Optics **17**, 538 (1978).
[18] K.-O. Peng and R. Marcel, Derivatives of transmittance and reflectance for an absorbing multilayer stack, Applied optics **24**, 501 (1985).
[19] A. Tikhonravov, Synthesis of optical coatings using optimality conditions, Vestnik MGU, physics and astronomy series **23**, 91 (1982).
[20] A. V. Tikhonravov, M. K. Trubetskov, and G. W. DeBell, Application of the needle optimization technique to the design of optical coatings, Applied optics **35**, 5493 (1996).
[21] R. H. Byrd, J. C. Gilbert, and J. Nocedal, A trust region method based on interior point techniques for nonlinear programming, Mathematical programming **89**, 149 (2000).
[22] R. H. Byrd, M. E. Hribar, and J. Nocedal, An interior point algorithm for large-scale nonlinear programming, SIAM Journal on Optimization **9**, 877 (1999).
[23] R. A. Waltz, J. L. Morales, J. Nocedal, and D. Orban, An interior algorithm for nonlinear optimization that combines line search and trust region steps, Mathematical programming **107**, 391 (2006).
[24] MATLAB, version R2020a, The MathWorks, Inc.